

REGULAR PAPER

Development of a neural probe integrated with high-efficiency MicroLEDs for in vivo application

To cite this article: Hiroki Yasunaga *et al* 2021 *Jpn. J. Appl. Phys.* **60** 016503

View the [article online](#) for updates and enhancements.

EXTENDED ABSTRACT DEADLINE: DECEMBER 18, 2020



239th ECS Meeting

with the 18th International Meeting on Chemical Sensors (IMCS)



May 30-June 3, 2021

SUBMIT NOW →



Development of a neural probe integrated with high-efficiency MicroLEDs for in vivo application

Hiroki Yasunaga¹, Toshihiro Takagi¹, Daisuke Shinko¹, Yusei Nakayama¹, Yuichi Takeuchi^{2,3}, Atsushi Nishikawa⁴, Alexander Loesing⁴, Masahiro Ohsawa³, and Hiroto Sekiguchi^{1,5*}

¹Department of Electrical and Electronic Information Engineering, Toyohashi University of Technology, Toyohashi, Aichi 441-8580, Japan

²MTA-SZTE "Momentum" Oscillatory Neuronal Networks Research Group, Department of Physiology, University of Szeged, Szeged 6720, Hungary

³Department of Neuropharmacology, Graduate School of Pharmaceutical Sciences, Nagoya City University, Nagoya, Aichi 467-8603, Japan

⁴ALLOS Semiconductors GmbH, Dresden 01237, Germany

⁵Japan Science and Technology, Precursory Research for Embryonic Science and Technology (PRESTO), Tokyo 102-0076, Japan

*E-mail: sekiguchi@ee.tut.ac.jp

Received September 23, 2020; revised November 25, 2020; accepted December 1, 2020; published online December 16, 2020

A neural probe with six micro-light-emitting diodes (MicroLEDs) and 15 neural electrodes was fabricated for optogenetic application. Local field potentials, which provide information about the neural activity, were successfully recorded using the neural probe, indicating the effectiveness of the neural electrodes. The MicroLEDs on the probe exhibited highly consistent current–voltage characteristics and sufficient light output of 20 mW mm⁻² at 1 mA to manipulate neural activity. The light distribution in brain tissue was simulated to estimate the optical stimulation area and a number of optically stimulated neurons. The increase in LED temperature, i.e. ΔT , was investigated because high temperatures can damage brain tissue. A curve illustrating the relationship between ΔT and the wall-plug efficiency was derived. The wall-plug efficiency was increased 1.8 times by installing an Ag mirror on the back of a MicroLED. These results suggest that the MicroLED neural probe would significantly contribute to the development of neuroscience research-purposed optogenetic technology. © 2020 The Japan Society of Applied Physics

1. Introduction

Advanced information processes, such as learning, memory, and recognition, are associated with higher brain functions and are the products of complex interactions between interconnected neurons, not by the function of single nerve cells. Thus, optogenetics research focused on cellular control has been attracting attention as an approach to understand such complex function mechanisms. Optogenetic technology uses light to precisely target specific cells for manipulation without affecting other cells in the brain.^{1–3} This technology contributes to elucidate how neural activity and animal behaviors are linked. Blue to blue-green emission is required for the Channelrhodopsin-2 (ChR2)-driven activation of neurons; however, the corresponding wavelength band is strongly influenced by how brain tissue scatters light. Thus, the development of photonic delivery technology that can transport light deep into the brain is required.

Although optical fibers can directly photoactivate target neurons with a high temporal resolution, and have been used to obtain a better understanding of the role of nerves in animal behavior,^{4–6} a new photodelivery device with a high spatiotemporal resolution is required to identify and control the functions of different nerves in a complex area where neurons with different functions are densely populated. Waveguide neural probes, which can simultaneously stimulate multiple regions while performing multicolor optical stimulation, have been proposed as a new type of device to fill this void.^{7–10} However, these types of probes are not designed to realize the high-resolution optical control of spatiotemporal neural activity patterns, which is necessary to clarify the depth-direction relationship between the six cortical layers. To achieve such highly precise optical control of complex neural activity, various researchers have developed micro-light-emitting diode (MicroLED) integration techniques that allow a large number of MicroLEDs to be mounted on a single neural probe.^{9–15} For example, a MicroLED neural probe has been developed by fabricating an epitaxial LED structure on a Si substrate, which was selected for its high processability. An LED

probe with 16 MicroLEDs was fabricated in one shank and it was reported to effectively activate neural activity in the depth direction in the cerebral cortex in vivo.¹⁵ This design allowed for the realization of complex neural activity manipulation; however, electrophysiological experiments require the use of neural recording electrodes to capture the manipulated neural activity.^{16–19} Because the LED probe and neural recording electrode probe are different, it is necessary to precisely control the position of each probe and insert both devices for observation. Thus, the development of an integrated MicroLED and neural recording electrode probe is essential. New optogenetic technology that enables the manipulation and recording of single neurons in the deep regions has been realized; however, there are a few reports of such integrated probes.^{20,21} Furthermore, among those that have been reported, they are not suitable for neuroscience research because the light output of MicroLEDs is as low as several μW because of their small size. Although an increase in the MicroLED size leads to an increase in light output, this size increase also lowers the spatial resolution and increases the amount of stimulation-induced heat, resulting in more heat damage. As such, it is necessary to optimize the trade-off between light output and device size; in addition, the installation of highly efficient LED devices that suppress Joule heat is required.

In this study, we developed a neural probe with six MicroLEDs and 15 neural recording electrodes on one shank. The neural activity in the brain tissue was observed by performing acute animal experiments using mice. The effects of the light output of the MicroLEDs on their spatial resolution and temperature under continuous operation were also investigated. Additionally, the wall-plug efficiency was increased by fabricating an Ag mirror structure on the back of each MicroLED.

2. Experimental methods

2.1. Fabrication of neural probe

The integrated neural probe was developed by fabricating a GaN-based LED structure with InGaN/GaN multi-quantum

wells ($\lambda = 460$ nm) on a (111) Si substrate (ALLOS Semiconductors GmbH).²²⁾ Figures 1(a) and 1(b) show the 3D schematic and cross-sectional structure of the integrated neural probe, which has MicroLEDs and neural electrodes. The probe was designed to have six MicroLEDs, each with a diameter of $50\ \mu\text{m}$, and 15 neural recording electrodes, each with an electrode area of $225\ \mu\text{m}^2$. The fabrication procedure is described as follows. A mesa structure was formed by implementing inductive coupled plasma-reactive ion etching for device separation. Subsequently, a transparent indium-tin-oxide (ITO) (600 nm) p-electrode was developed by using an electron beam (EB) evaporator and performing an annealing process under an oxygen atmosphere, followed by the deposition of a Ti/Al/Ti/Au (80 nm/80 nm/150 nm/50 nm) n-electrode. A permanent SU-8 epoxy photoresist coating was also applied as an interlayer insulation film. An EB evaporator was used to deposit a Ti/Au (250 nm/50 nm) metal wiring layer to connect the MicroLEDs and enable individual MicroLED activation. The width of the metal wiring on the face of the probe was designed to be $5\ \mu\text{m}$. Next, another SU-8 photoresist coating was applied as an insulating layer between the metal wiring layer of the MicroLEDs and neural electrodes. Then, Ti/Pt (40 nm/10 nm) neural electrodes were deposited by using an EB evaporator. A biocompatible SU-8 layer was then deposited to ensure that only the front face of each electrode was exposed to the environment. Lastly, a deep reactive ion etching technique was applied to process the LED chip into a needle shape structure and ensure smooth insertion into the brain tissue. The probe length, width, and thickness were designed to be 4 mm, $170\ \mu\text{m}$, and $300\ \mu\text{m}$, respectively. The integrated probe was mounted on a PCB board with a compact design of $12.6\ \text{mm} \times 10\ \text{mm}$, as shown in Fig. 1(c). Because the mass after device mounting was as low as approximately 0.16 g, the burden on the animal was

expected to be minimal. Figure 1(d) shows optical microscope images of the developed neural probe before and during LED operation. The MicroLEDs can be individually activated, and blue emission was observed from each MicroLED. The current–voltage (I – V) characteristics were evaluated with voltage sweep by semiconductor parameter analyzer (B1500A, Keysight). External quantum efficiency (EQE) and wall-plug efficiency measurements were carried out at room temperature with a current sweep, which led to overheating, by positioning a wavelength sensitivity corrected optical power meter (82313B, ADCMT) on top of the MicroLED sample.

To investigate the characteristics of the neural electrode, a simple probe with only the neural electrodes was prepared by only implementing the electrode fabrication process of the above-described probe fabrication method. The impedance of each neural electrode was measured by immersing the neural probe in saline and employing an impedance analyzer.

2.2. Animal study

All of the experimental protocols for animal studies were approved by the Animal Care and Use Committee of Nagoya City University, and carried out in accordance with the guidelines of the National Institutes of Health, and the Japanese Pharmacological Society. C57BL6 mice were anesthetized with $1.2\ \text{g kg}^{-1}$ urethane (i.p.). They were then mounted on a stereotaxic instrument. The lack of a nociceptive reflex was confirmed throughout the surgical procedure to ensure that general anesthesia was maintained. Each animal's rectal temperature was maintained at $36\ ^\circ\text{C}$ – $37\ ^\circ\text{C}$. The head position was adjusted such that the bregma and lambda were at the same level. A small cranial window was made over the somatomotor cortex. The neural electrode probe was perpendicularly inserted into the brain by the 1.00 mm below the surface of the dura mater. The position of the probe was then maintained for 20–30 min to ensure that it was stabilized before being gently advanced to approximately 2 mm below the surface of the dura mater. The probe was connected to a 32-channel headstage (C3314, Intan Technologies, Los Angeles, CA) via a nano connector (A79026-001, Omnetics Connector Corporation, Minneapolis, MN), amplified by 192 times, and then digitized at 20 kHz. The multiplexed signals were acquired by using an Open Ephys acquisition board before being stored on a PC.

The wide-band signals were first down-sampled to 1250 samples/s offline. They were then filtered by applying a 3rd-order zero-phase lag Butterworth filter to obtain the local field potentials (LFPs) and spike signals that were within the ranges of 1–625 Hz and 500–3000 Hz, respectively. All data were analyzed using the MATLAB platform (RRID:SCR_001622; Mathworks, Natick, MA, USA) unless otherwise noted.

2.3. Simulation of light scattering

The simulations were performed under the conditions of light with a wavelength of 460 nm. A finite-difference time-domain method was employed in electromagnetic field analysis to confirm that a Lambertian distribution could be obtained. Because brain tissue tends to scatter light, the Monte Carlo method was used to simulate light propagation through brain tissue. The scattering coefficient, anisotropy factor, and absorption coefficient for the gray brain matter were $\mu_s = 105\ \text{cm}^{-1}$, $g = 0.88$, and $\mu_a = 0.6\ \text{cm}^{-1}$, respectively.²³⁾

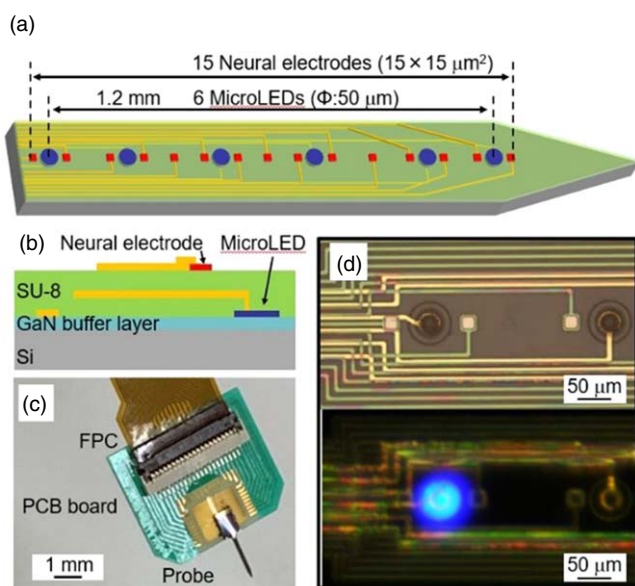


Fig. 1. (Color online) (a) 3D schematic and (b) cross-sectional structure of the proposed integrated MicroLED and neural electrode probe. The probe has six MicroLEDs, each with a diameter of $50\ \mu\text{m}$, and 15 Ti/Pt neural electrodes, each with an electrode area of $225\ \mu\text{m}^2$. (c) Photograph of a MicroLED neural probe mounted on a PCB board ($12.6\ \text{mm} \times 10\ \text{mm}$) connected to a flexible printed circuit (FPC) board. (d) Optical microscope images of a neural probe before and during LED operation.

3. Results and discussion

3.1. Characterization of neural electrodes

The characteristics of the neural electrodes were investigated. The impedances were as small as approximately 600 kΩ at 200 Hz, and 100 kΩ at 1 kHz, respectively. This is noteworthy because a lower electrode impedance corresponds to smaller electromagnetic interference artifacts.²¹⁾ More specifically, the electrode impedance decreased with increasing frequency because the capacitance component at the interface between the electrode and saline solution decreased with increasing frequency. Acute electrophysiological recording was performed to observe the neural activity in anesthetized mice. Figure 2(a) shows an illustration of the animal study using a neural electrode. The neural electrode probe was smoothly inserted into the brain tissue. Figure 2(b) shows an example of the LFPs of neurons, as recorded by the 15-channel neural electrode probe. As can be seen, LFP signals were obtained from all of the neural electrodes. The neural probe also detected neural spikes corresponding to the action potentials of individual neurons (not shown here). This suggests that the fabricated neural electrode is an effective device for neural activity recording.

3.2. Characterization of MicroLEDs

Next, the electrical and optical properties of the MicroLEDs on the integrated neural probe were evaluated. Figure 3(a) shows the I - V characteristics of three representative MicroLEDs. The corresponding rectified voltage curves were found to be highly consistent, confirming a turn-on voltage of 3.2 V. Additionally, blue emission, with a peak wavelength of 460 nm, was observed. Figure 3(b) shows the current-light output (I - L) and efficiency droop curves for the representative MicroLEDs. A light output of 19.3 mW mm⁻², which corresponded to 38 μW, was obtained at 1 mA with an EQE of 1.4%. Because the input power that cannot be extracted for light emission is converted to heat, emission efficiency must be prioritized for animal experimentation. Even a slight temperature increase, e.g. approximately 1 °C, can alter neural network functionality or damage brain tissue. Thus, it is necessary to know how much heat is generated by the MicroLEDs before implementing the probe in an animal experiment. Before evaluating the extent of device heating, we determined the MicroLED light output required for the animal experiment. A light output of 1 mW mm⁻² has been reported to be required ChR2 activation.^{24,25)} To approximate the relationship between the light output and the number of

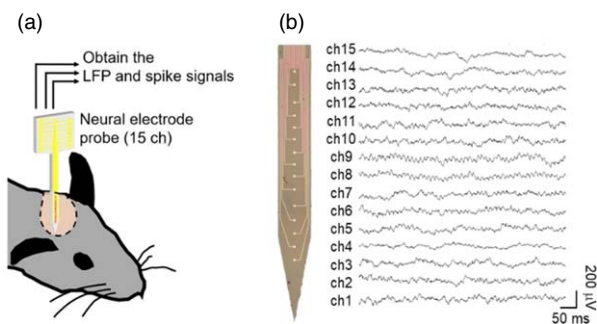


Fig. 2. (Color online) (a) Illustration showing the procedure for inserting the neural electrode probe into the cortical tissue of a mouse. (b) Enlarged photograph of the 15-channel neural electrode probe, and local field potentials (LFPs) recorded from neurons.

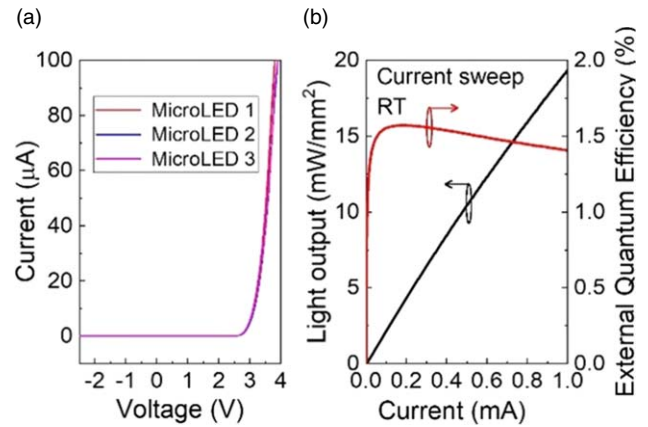


Fig. 3. (Color online) (a) Current-voltage (I - V) curve for three representative MicroLEDs. (b) Current-light output (I - L) and efficiency droop curves at RT for one of the representative MicroLEDs. The light output was 19.3 mW mm⁻² at 1 mA (50 A cm⁻²) with an EQE of 1.4%.

stimulated neurons, how the device distributes light throughout brain tissue was simulated by electromagnetic field analysis and the Monte Carlo method. The light distribution is also important from the perspective of spatial resolution because the spatial resolution of a MicroLED probe is not only determined by the MicroLED size, but also by the scattering of the light from each MicroLED. For the radiation characteristics of MicroLEDs, a Lambertian distribution could be obtained by electromagnetic field analysis, even under the conditions of a MicroLED with a diameter of 50 μm. When the angle-resolved electroluminescence measurement was performed in ambient air, the result was nearly the same as the corresponding simulated result. Figure 4 shows the results of using the Monte Carlo method to simulate how the light from one MicroLED with a diameter of 50 μm is scattered through brain tissue. The white lines denote the areas where the light spreads to 1 mW mm⁻² at each light output on the MicroLED surface. As can be seen, increasing the light output increased the number of optically stimulated neurons. It has been reported that the average density of neurons is 9.2 × 10⁴ per mm.^{3,26)} Thus, the numbers of neurons stimulated by 5, 10, 20, 50, and 100 mW mm⁻² were roughly estimated to be 5, 12, 25, 120, and 320 neurons, respectively. It should also be noted that the number and area of neurons that can be stimulated vary according to the target brain region.

Next, the extent of increase in MicroLED temperature under the conditions of continuous operation was investigated by using an uncooled thermal imaging camera (FLIR A325sc). Figure 5(a) shows the temperature increase (ΔT) as a function of current. The wall-plug efficiency of the MicroLED was approximately 0.8% at 1 mA. ΔT monotonically increased from 0.35 °C to 5.2 °C as the current was increased from 0.5 to 5.0 mA. Under the assumption that all energy that is not used to emit light is converted to heat, the extent of temperature increase is determined by the input power and wall-plug efficiency. Considering how light was determined to scatter throughout the surrounding brain tissue, a MicroLED activation energy of 1 mW mm⁻² and consequently enable optical control of specific neural activity.^{2,23)} Thus, the temperature change can be suppressed within 1 °C for such an output level. In addition to an increase in

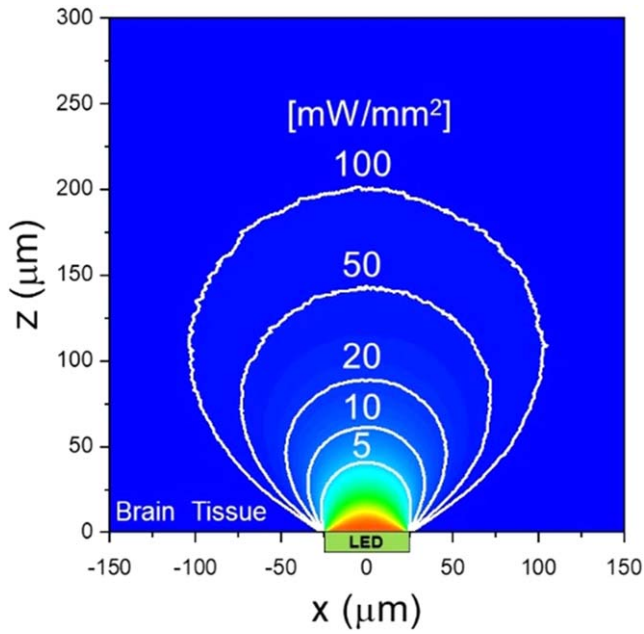


Fig. 4. (Color online) Results of Monte Carlo simulation of light propagating from one MicroLED with a diameter of $50\ \mu\text{m}$ through cortical tissue. The white lines denote the areas in which the scattered light corresponds to an irradiance of $1\ \text{mW}\ \text{mm}^{-2}$ for MicroLED surface light output values of 5, 10, 20, 50, and $100\ \text{mW}\ \text{mm}^{-2}$.

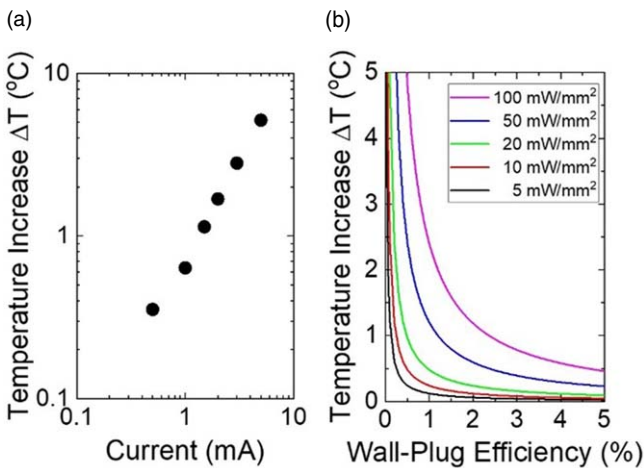


Fig. 5. (Color online) (a) Temperature increase, ΔT , as a function of current. The wall-plug efficiency of the MicroLED was approximately 0.8% at 1 mA. ΔT monotonically increased from $0.35\ ^\circ\text{C}$ to $5.2\ ^\circ\text{C}$ as the current was increased from 0.5 to 5 mA. (b) ΔT as a function of wall-plug efficiency for light outputs of 5, 10, 20, 50, and $100\ \text{mW}\ \text{mm}^{-2}$.

MicroLED temperature, the influence of light absorption on the brain tissue temperature should be considered. Considering based on the theoretical formula of the extent of increase in living body temperature caused by laser irradiation described in Ref. 27, it was estimated that the temperature only increased below $0.01\ ^\circ\text{C}$ even with a light power of $100\ \text{mW}\ \text{mm}^{-2}$ because light output of MicroLED was sufficiently weak compared with that of the lasers. Therefore, the temperature in the brain tissue is determined by the MicroLED temperature. When employing the proposed integrated probe to regulate local neural activity for the purpose of clarifying the spatiotemporal correlations, the temperature increase can be further suppressed because the optical stimulation delivered by each MicroLED amounts to a

pulse stimulation with a duration of several milliseconds to several tens of milliseconds. Although it is expected that the wall-plug efficiency changes due to pulse operation, the efficiency hardly changes because MicroLED is operated with low current region due to suppression of thermal effects on the brain tissue. In fact, the wall-plug efficiency did not change with changing the duty ratio from 0.1% to 100%. On the other hand, in in vivo animal experiments, it is necessary to optically stimulate a wider area, which, depending on the brain region, may require a longer duration of stimulation. Thus, the wall-plug efficiency must be increased to reduce the device temperature at high light output. It is also necessary to clarify the relationship between temperature change and wall-plug efficiency. Figure 5(b) shows the temperature change curve as a function of wall-plug efficiency for each light output level. The temperature increase was derived from the experimental power consumption data shown in Fig. 5(a) under the assumption that the wall-plug efficiency is not dependent on the current. It can be seen that high wall-plug efficiency led to lower temperature increase; this is because high levels of light output can be achieved with low input power consumption. As shown in Fig. 5(b), at $20\ \text{mW}\ \text{mm}^{-2}$, a wall-plug efficiency of 0.8% was associated with a $0.6\ ^\circ\text{C}$ temperature increase. However, at $100\ \text{mW}\ \text{mm}^{-2}$, the temperature increase can remain below $1.0\ ^\circ\text{C}$ if a wall-plug efficiency of at least 3.0% can be achieved. The combination of high output and low wall-plug efficiency is the result of a high driving current; these conditions lead to relatively higher temperature increases because ΔT is strongly affected by efficiency droop,^{28–31} as shown in Fig. 3(b). Thus, researchers in the neuroscience field should prioritize increasing the wall-plug efficiency. The wall-plug efficiency of the fabricated MicroLEDs was measured to be 0.8%, which, considering the signal loss in the current system, is reasonable. Furthermore, the wall-plug efficiency could be increased by optimizing the process design and customizing the MicroLED epitaxial structure of the device design. To this end, we attempted to increase the efficiency by fabricating a mirror directly under each MicroLED.

3.3. Fabrication of Ag mirror on the backside of MicroLED

A schematic diagram of the MicroLED structure with an Ag mirror is presented as the Fig. 6 inset. After fabricating the MicroLED, the Si substrate under the MicroLED was etched by employing a deep reactive ion etching technique. Then, an Ag mirror (200 nm) was deposited on the back of MicroLED by using an EB evaporator. With this structure, the light output at the upper face of the MicroLED is higher because the Si substrate suppresses light absorption while the Ag mirror reflects light. Figure 6 illustrates the I - L characteristics of MicroLEDs with and without the Ag mirror. The light output was found to increase with increasing current. However, the MicroLED with the Ag mirror was associated with light output that was approximately twice that of the MicroLED without the Ag mirror. Furthermore, a light output of approximately $90\ \text{mW}\ \text{mm}^{-2}$ was obtained at 3 mA, and the wall-plug efficiency was 1.4%, corresponding to an increase of approximately 1.8 times the corresponding value for the MicroLED without the Ag mirror. Thus, under the condition of continuous LED operation, the increase in

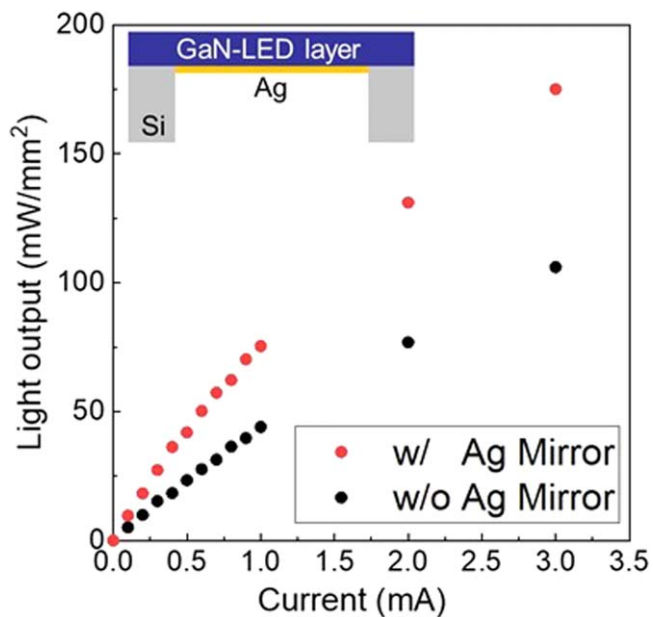


Fig. 6. (Color online) I - L curve for MicroLEDs with and without an Ag mirror. Inset: schematic of the MicroLED structure with an Ag mirror.

temperature of the MicroLED with the Ag mirror would be less than half that of the MicroLED without the Ag mirror. These results represent a foundational step toward the realization of an integrated MicroLED neural probe for the optogenetic optical stimulation of relatively large volumes of cortical tissue. Regarding its applicability in the field of neuroscience, it is important that the LED operation in cortical tissue be highly reliable; additionally, the development of biocompatible coating technology for the device surface is required.

4. Conclusions

A neural probe integrated with six MicroLEDs and 15 neural recording electrodes was fabricated for optogenetic application. LFPs and neural spike signals were successfully recorded from the cortical tissue of mice, indicating the effectiveness of the neural electrodes. Next, the properties of the MicroLEDs fabricated on the neural probe were evaluated. The MicroLEDs exhibited highly consistent I - V characteristics, and each had a light output of approximately 20 mW mm^{-2} , and EQE of 1.4% at 1.0 mA. Additionally, the light distribution in cortical tissue was simulated to estimate the optically stimulated area and a number of optically stimulated neurons. When the temperature increase of MicroLEDs under continuous operation was evaluated, the temperature was found to increase from $0.35 \text{ }^\circ\text{C}$ to $5.2 \text{ }^\circ\text{C}$ as the current was increased from 0.5 to 5.0 mA. These results were used to quantify the relationship between temperature increase and wall-plug efficiency, which may be used as a reference for the future development of MicroLED optogenetic technology purposed for neuroscience research. Lastly, the wall-plug efficiency was found to be increased by fabricating an Ag mirror on the back of the MicroLED.

These results suggest that the developed neural probe would be useful as a tool for in vivo optogenetics research.

Acknowledgments

This work was partially supported by The Precursory Research for Embryonic Science and Technology Agency (JPMJPR1885), Research Foundation for OptoScience and Technology, and The Nitto Foundation. All device fabrication processes were carried out using the facility of the Electronics-Inspired Interdisciplinary Research Institute (EIIRIS), and the Venture Business Laboratory, Toyohashi University of Technology.

- 1) K. Deisseroth, G. Feng, A. K. Majewska, G. Miesenböck, A. Ting, and M. J. Schnitzer, *J. Neurosci.* **26**, 10380 (2006).
- 2) K. Deisseroth, *Nat. Method.* **8**, 26 (2011).
- 3) T. Ishizuka, M. Kakuda, R. Araki, and H. Yawo, *Neurosci. Res.* **54**, 85 (2006).
- 4) D. Lin, M. P. Boyle, P. Dollar, H. Lee, E. S. Lein, P. Perona, and D. J. Anderson, *Nature* **470**, 221 (2011).
- 5) X. Liu, S. Ramirez, P. T. Pang, C. B. Puryear, A. Govindarajan, K. Deisseroth, and S. Tonegawa, *Nature* **484**, 381 (2012).
- 6) H. Watanabe, H. Sano, S. Chiken, K. Kobayashi, Y. Fukata, H. Mushiaka, and A. Nambu, *Nat. Commun.* **11**, 3253 (2020).
- 7) K. Kampasi, D. F. English, J. Seymour, E. Stark, S. McKenzie, M. Vöröslakos, G. Buzsáki, K. D. Wise, and E. Yoon, *Microsyst. Nanoeng.* **4**, 10 (2018).
- 8) K. Y. Kwon and W. Li, Proc. IEEE Int. Conf. on Micro Electro Mechanical Systems (MEMS) 1017, 2013.
- 9) Y. Son, H. J. Lee, J. Kim, H. Shin, N. Choi, C. J. Lee, E.-S. Yoon, K. D. Wise, T. G. Kim, and I.-J. Cho, *Sci. Rep.* **5**, 15466 (2015).
- 10) H. Sekiguchi, H. Yasunaga, K. Tsuchiyama, and R. Nitta, *Electron. Lett.* **55**, 619 (2019).
- 11) T.-I. Kim et al., *Science* **340**, 211 (2013).
- 12) N. McAlinden, D. Massoubre, E. Richardson, E. Gu, S. Sakata, M. D. Dawson, and K. Mathieson, *Opt. Lett.* **38**, 992 (2013).
- 13) C. Göbner, C. Bierbrauer, R. Moserl, M. Kunzer, K. Holc, W. Pletschen, K. Köhler, J. Wagner, M. Schwaerzle, and P. Ruther, *J. Phys. D: Appl. Phys.* **47**, 205401 (2014).
- 14) E. Klein, C. Gossler, O. Paul, and P. Ruther, *Front. Neurosci.* **12**, 659 (2018).
- 15) R. Scharf, T. Tsunematsu, N. McAlinden, M. D. Dawson, S. Sakata, and K. Mathieson, *Sci. Rep.* **6**, 28381 (2016).
- 16) K. C. Cheung, K. Djupsund, Y. Dan, and L. P. Lee, *J. Microelectromech. Syst.* **12**, 179 (2003).
- 17) P. Norlin, M. Kindlundh, A. Mouroux, K. Yoshida, and U. G. Hofmann, *J. Micromech. Microeng.* **12**, 414 (2002).
- 18) M. HajjHassan, V. Chodavarapu, and S. Musallam, *Sensors* **8**, 6704 (2008).
- 19) P. Ruther et al., *Biomed. Tech.* **53**, 240 (2008).
- 20) F. Wu, E. Stark, P.-C. Ku, K. D. Wise, G. Buzsáki, and E. Yoon, *Neuron* **88**, 1136 (2015).
- 21) K. Kim, M. Vöröslakos, J. P. Seymour, K. D. Wise, G. Buzsáki, and E. Yoon, *Nat. Commun.* **11**, 2063 (2020).
- 22) B. Sliszhka, A. Nishikawa, and A. Loesing, *Semiconductor Today* **15**, 48 (2020).
- 23) A. N. Yaroslavsky, P. C. Schulze, I. V. Yaroslavsky, R. Schober, F. Ulrich, and H.-J. Schwarzmaier, *Phys. Med. Biol.* **47**, 2059 (2002).
- 24) E. Stark, T. Koos, and G. Buzsáki, *J. Neurophysiol.* **108**, 349 (2012).
- 25) N. Grossman et al., *J. Neural Eng.* **7**, 016004 (2010).
- 26) A. Schüz and G. Palm, *J. Comp. Neurol.* **286**, 442 (1989).
- 27) P. E. Dyer, *Proc. SPIE* **3092**, 412 (1997).
- 28) M.-H. Kim, *Appl. Phys. Lett.* **91**, 183507 (2007).
- 29) J. Piprek, *Phys. Status Solidi A* **207**, 2217 (2010).
- 30) G. Verzellesi, D. Saguatti, M. Meneghini, F. Bertazzi, M. Goano, G. Meneghesso, and E. Zanoni, *J. Appl. Phys.* **114**, 071101 (2013).
- 31) V. A. Jhalani, J.-J. Zhou, and M. Bernardi, *Nano Lett.* **17**, 5012 (2017).